




## Cucurbiturils brighten Au nanoclusters in water†

Cite this: *Chem. Sci.*, 2020, 11, 3531Tao Jiang, Guojuan Qu, Jie Wang,  Xiang Ma \* and He Tian

All publication charges for this article have been paid for by the Royal Society of Chemistry

Gold nanoclusters (AuNCs) with well-defined atomically precise structures present promising emissive prospects for excellent biocompatibility and optical properties. However, the relatively low luminescence efficiency in solutions for most AuNCs is still a perplexing issue to be resolved. In this study, a facile supramolecular strategy was developed to rigidify the surface of FGGC-AuNCs by modifying transition rates in excited states *via* host-guest self-assembly between cucurbiturils (CBs) and FGGC (Phe-Gly-Gly-Cys peptide). In aqueous solutions, CB/FGGC-AuNCs presented an extremely enhanced red phosphorescence emission with a quantum yield (QY) of 51% for CB[7] and 39% for CB[8], while simple FGGC-AuNCs only showed a weak emission with a QY of 7.5%. Furthermore, CB[7]/FGGC-AuNCs showed excellent results in live cell luminescence imaging for A549 cancer cells. Our study demonstrates that host-guest self-assembly assisted by macrocycles is a facile and effective tool to non-covalently modify and adjust optical properties of nanostructures on ultra-small scales.

Received 26th January 2020  
Accepted 6th March 2020

DOI: 10.1039/d0sc00473a

rsc.li/chemical-science

## Introduction

Host-guest self-assembly, typically the encapsulation behavior between small motifs and macrocycle molecules bearing cavities with a certain size, has received extensive attention in molecular recognition and stimuli-responsive systems.<sup>1–8</sup> Remarkably, driven by multiple non-covalent interactions such as ion-dipole, hydrophobic and H-bonding effects, macrocyclic cucurbit[*n*]urils (CB[*n*], *n* = 5–8, typically) exhibit a robust binding strength with elaborately tailored guests to form stable binary and ternary host-guest complexes in aqueous solutions.<sup>9,10</sup> In the past two decades, the advancements in CB[*n*]-based host-guest self-assembly have greatly facilitated the design of functional materials ranging from single molecules to various nanostructures.<sup>11–15</sup> Contributing to the abundant recognition sites on surfaces, nanoparticles have been extensively integrated with host-guest self-assembly to obtain additional surprising functions.<sup>16–18</sup> Nevertheless, less attention has been paid to ultrasmall nanostructures below 3 nm such as metal nanoclusters (such as Ag, Cu and Au nanoclusters) due to the difficulty in tailoring an appropriate nanostructure with desirable properties and host-guest recognition capability. Significantly, metal nanoclusters which fill the gap between single atoms and bulk nanostructures present disparate microscopic structures and macroscopic properties. In particular, thiolate-protected gold nanoclusters (AuNCs),<sup>19</sup> which

have atomically precise compositions (Au<sub>*x*</sub>(SR)<sub>*y*</sub>, where *x* and *y* have exact values, SR = thiolate ligands), have emerged as promising emissive and catalytic materials due to the intriguing optical and photoelectrical properties.<sup>20–26</sup> Different from common gold nanoparticles, AuNCs don't present a surface plasmon resonance (SPR) effect but show a unique Au(0) kernel-Au(I) shell structure with discrete energy levels, endowing AuNCs with full spectrum photoluminescence emission from blue to NIR as quantum dots and organic dyes.<sup>27–29</sup> Besides, the outstanding photo-stability, long carrier lifetime and Stokes shift, and efficient renal clearance properties make AuNCs ideal choices for analysis and bio-imaging.<sup>30,31</sup> On the other hand, the relatively weak luminescence and hardly adjustable emission have been a non-negligible hindrance to practical applications.<sup>32</sup>

To date, the specific luminescence mechanism of AuNCs has remained controversial. Researchers still debate the photoluminescence origin between the Au(0) kernel and Au(I) shell.<sup>33</sup> Nevertheless, it has been clearly demonstrated that suppression of kernel relaxation and surface vibrations is crucial for enhancing the emission intensity of AuNCs.<sup>33–39</sup> Still, approaches based on this principle tend to be less facile for enhancing the emission, and reports on the photoluminescence with a QY beyond 15% especially in aqueous solutions remain scarce.<sup>32</sup> In this respect, CB[*n*]-assisted host-guest self-assembly is probably an ideal choice to mediate the emission of AuNCs. The abundant ligands on the surfaces are closely related to the luminescence intensity of AuNCs and also offer extensive feasibility for incorporation with cucurbiturils. Herein, we developed a CB[*n*]-assisted (*n* = 7, 8) self-assembly strategy to reversibly brighten and adjust the red emission from Au<sub>22</sub>(-FGGC)<sub>18</sub> nanoclusters using CB-FGGC (FGGC = N-terminal Phe-Gly-Gly-Cys peptide) recognition to rigidify the surface of

Key Laboratory for Advanced Materials, Feringa Nobel Prize Scientist Joint Research Center, Institute of Fine Chemicals, School of Chemistry and Molecular Engineering, East China University of Science & Technology, 130 Meilong Road, Shanghai, 200237, China. E-mail: maxiang@ecust.edu.cn

† Electronic supplementary information (ESI) available. See DOI: 10.1039/d0sc00473a



FGGC-AuNCs in aqueous solutions. The FGGC fragment on FGGC peptide served as a binding site for CB[7] and CB[8], and the cysteine fragment was essential to forming the compressed Au(I)-thiolate surface of AuNCs. The rigidity and outstanding binding ability allow cucurbiturils to act as firm but detachable “shackles” for capped ligands. This supramolecular approach was demonstrated to effectively enhance the radiative transition rate and suppress the non-radiative rate simultaneously. As a result, the luminescence QY of supramolecular FGGC-AuNCs was up to 51% for CB[7] and 39% for CB[8] in aqueous solutions at room temperature, while the simple FGGC-AuNCs exhibited a relatively low QY of 7.5% under the same conditions (Scheme 1). Due to the excellent optical properties, CB[7]/FGGC-AuNCs exhibited excellent luminescence imaging for cancer A549 cells as well.

## Results and discussion

### Identification of $\text{Au}_{22}(\text{FGGC})_{18}$ nanoclusters

The red luminescent FGGC-AuNCs were synthesized through  $\text{NaBH}_4$  reduction methods and separated by preparative thin-layer chromatography (PTLC, see the ESI† for details).

High-Resolution Transmission Electron Microscopy (HRTEM) images showed an ultra-small size below 2 nm of Au nanoclusters (see Fig. S1†). Moreover, the chemical composition of isolated nanoclusters was indicated to be  $\text{Au}_{22}(\text{FGGC})_{18}$  by Electrospray Ionization Mass Spectrometry (ESI-MS) in positive polarity mode. As shown in Fig. S2,† the most intense peaks at  $m/z \sim 1867.3$  Da and 2240.8 Da in the experimental isotope pattern are consistent with the species of  $[\text{Au}_{22}(\text{FGGC})_{18}]^{6+}$

(calculated: 1867.1) and  $[\text{Au}_{22}(\text{FGGC})_{18} + 5\text{H}]^{5+}$  (calculated: 2240.3), respectively. As shown in Fig. 1, the excitation, absorption and photoluminescence spectra show a maximum  $\lambda_{\text{abs}}$  at 515 nm and  $\lambda_{\text{em}}$  at 665 nm for FGGC-AuNCs in aqueous

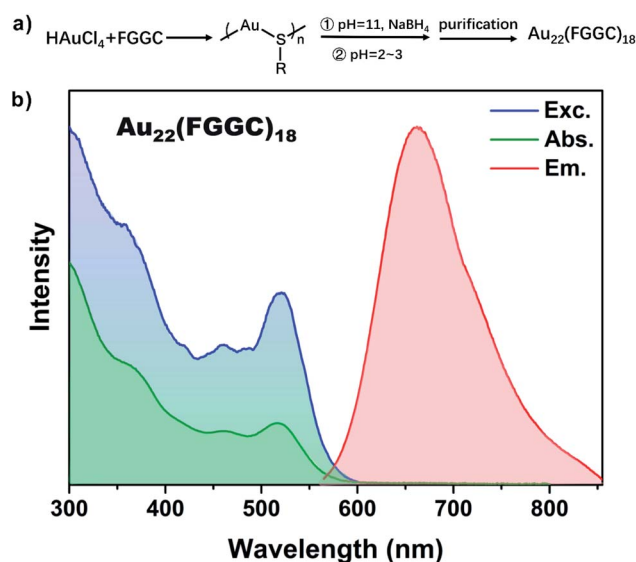
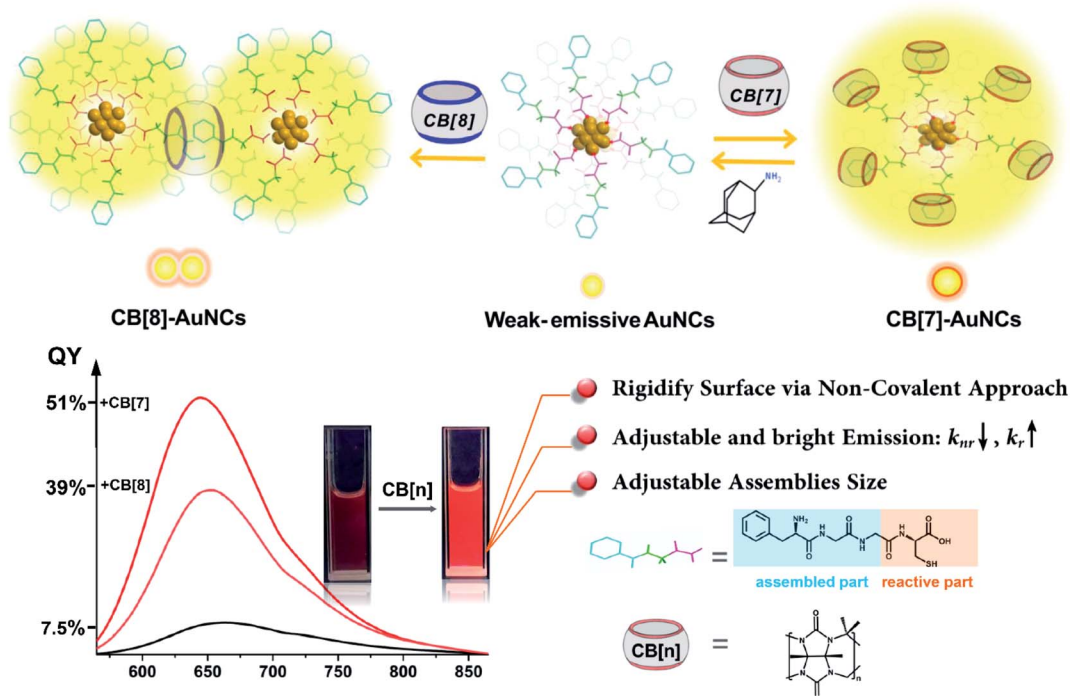


Fig. 1 (a) Synthesis procedure of  $\text{Au}_{22}(\text{FGGC})_{18}$  nanoclusters. Inset: molecular structure of FGGC peptide. R stands for the FGGC unit without the thiol group. (b) Excitation spectrum (blue curve), UV-Vis absorption spectrum (green curve) and emission spectrum (red curve) of  $\text{Au}_{22}(\text{FGGC})_{18}$  nanoclusters in aqueous solutions. The emission spectrum was determined at an excitation wavelength of 515 nm and the excitation spectrum was recorded at 665 nm.



Scheme 1 Schematic diagram of host-guest assembly of CB[7] and CB[8] with FGGC-AuNCs and the corresponding luminescence photographs.



solutions, which coincide with the data reported in previous literature.<sup>40</sup> According to the corresponding accurate simulation for Au<sub>22</sub>(SR)<sub>18</sub> proposed in previous studies,<sup>41,42</sup> the Au<sub>22</sub>(-FGGC)<sub>18</sub> probably possesses a structure consisting of a Au<sub>7</sub> kernel surrounded by a [Au<sub>6</sub>(FGGC)<sub>6</sub> Au(I) complex and three Au<sub>3</sub>(FGGC)<sub>4</sub> staple motifs. The abundant surface ligands provide ample space for host-guest self-assembly.

### Host-guest assembly of FGGC peptide with cucurbiturils

To simplify the self-assembly interaction between the surface ligands of FGGC-AuNCs and CB[n], an isolated FGGC peptide was selected to investigate the host-guest interactions. It is reported that the CB[8]/FGGC complex adopts a 1:2 host-guest binding motif with an extremely large  $K_a$  as large as  $10^{12} \text{ M}^{-2}$  in aqueous solutions ascribed to the large cavity of CB[8].<sup>43,44</sup> Unlike CB[8], our study demonstrated that CB[7] could include only one FGGC peptide in aqueous solutions due to its smaller hydrophobic cavity. Fig. 2 shows the <sup>1</sup>H Nuclear Magnetic Resonance (NMR) signal variations of FGGC peptide upon addition with different ratios of CB[7] in deuterium oxide solvents; the NMR signals of FGGC peptide protons are remarkably shifted at increasing ratios from 0 to 1.0 of CB[7]. Protons **a-d** on the phenylalanine unit exhibit a considerable upfield shift due to the shielding effect from the cavity of CB[7]. More specifically, the proton signals of **a** and **b** (*m*, 7.22–7.33 ppm) are gradually split into two triplet peaks at 6.62 ppm and 6.48 ppm, respectively; moreover, proton **d** transforms the dd peak at 3.10 ppm into a slightly upfield shifted dd peak at 3.01 ppm and a remarkably upfield shifted triple peak at 2.51 ppm. This result is due to the rotation restriction of the Phe fragment in the cavity of CB[7] and thus the adjacent proton **e**

exhibits an apparent chiral effect. Conversely, protons **e**, **f**, and **g** present a slightly downfield shift, which is attributed to the external deshielding effect from the macrocycle. Simply put, the NMR signal variations of FGGC peptide indicate a 1:1 encapsulation of the phenylalanine unit into the cavity of the host, revealing spatial interaction between the glycine-glycine fragment and the portal of CB[7]. Additionally, Isothermal Titration Calorimetry (ITC) measurements of the FGGC/CB[7] supramolecular assembly in a pH = 7.0 aqueous solution at 298 K have also been performed to probe the thermodynamic nature of the host-guest binding. As shown in Fig. S3,† a binding constant  $K_a$  was recorded as large as  $2 \times 10^6 \text{ M}^{-1}$  in the 1:1 binding motif, indicating the formation of fairly stable binary complexes between FGGC and CB[7] in aqueous solutions. On the other hand, the host CB[6] could hardly assemble with FGGC peptide due to its cavity being too small to encapsulate the phenylalanine unit as indicated by the NMR results in Fig. S4.†

### Enhanced emission of CB/FGGC-AuNC assemblies

The high affinity of FGGC peptide to CB[7] and CB[8] offers a precondition for fabricating supramolecular capped ligands for FGGC-AuNCs. As shown in Fig. 3, both CB[7] and CB[8] FGGC-AuNC assemblies exhibit extremely enhanced red luminescence in aqueous solutions. Fig. 3a indicated an extremely enhanced emission of FGGC-AuNCs accompanied by a slight

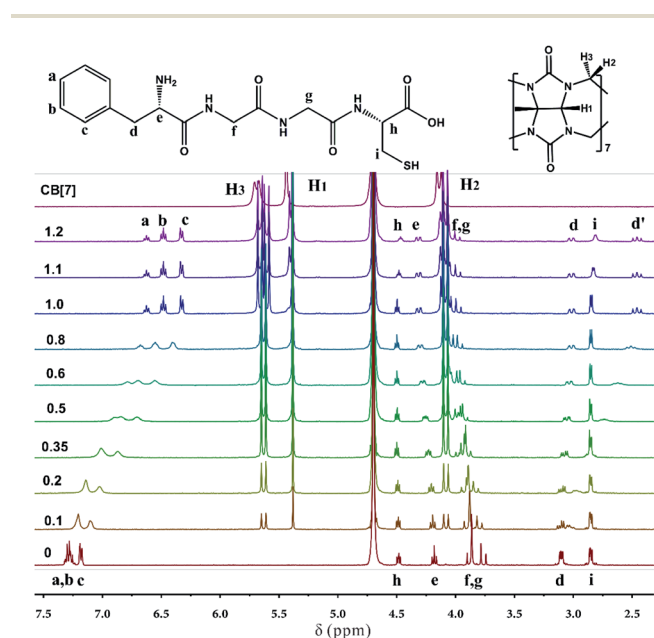


Fig. 2 <sup>1</sup>H NMR spectra of FGGC peptide with different ratios of CB[7] in D<sub>2</sub>O. The concentration of FGGC is 2 mM in D<sub>2</sub>O. The numbers on the left stand for the molar ratios of CB[7]/FGGC; characters **a-i** and H<sub>1</sub>-H<sub>3</sub> represent the protons on FGGC and CB[7].

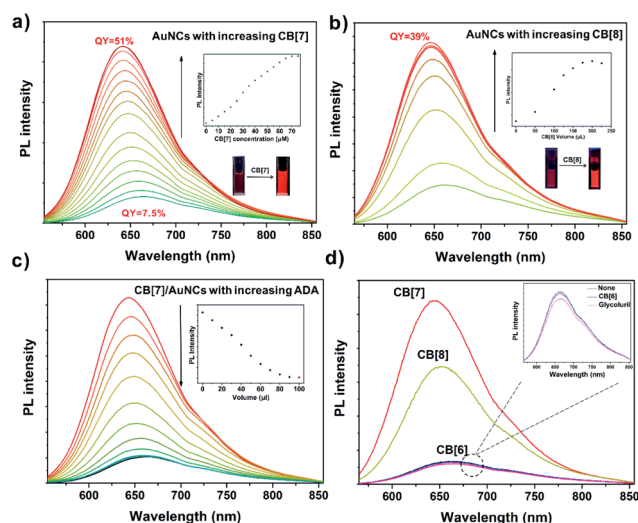


Fig. 3 Photoluminescence spectra of FGGC-AuNCs with increasing concentrations of CB[7] (a) and CB[8] (b) in aqueous solutions. Inset: the associated maximum emission trace of PL (photoluminescence) spectra and photographs of FGGC-AuNCs before (left) and after (right) adding CBs under 365 nm light. The red labels represent the lowest and highest photo-luminescence quantum yield of FGGC-AuNCs. (c) Photoluminescence spectra of CB[7]/FGGC-AuNCs (2 mL, the absorbance at 515 nm is 0.05) with different volumes of ADA (1 mM) in aqueous solutions. Inset: the associated maximum emission trace of PL spectra. The black curve and red dot represent the PL intensity of FGGC-AuNCs free of CB[7]. (d) Photoluminescence spectra of FGGC-AuNCs and FGGC-AuNCs with glycoluril (7 mM), CB[6], CB[7] and CB[8] in aqueous solutions. The concentration of CB[n] is 1 mM. All photoluminescence spectra in the figure were obtained at an excitation wavelength of 515 nm.



blueshift in aqueous solutions when adding increasing amounts of CB[7]. In addition, the emission enhancement is an immediate process due to the ultrafast host-guest recognition between FGGC peptide and CB[7] in water (see Movie S1†). Notably, the supramolecular CB[7]/FGGC-AuNCs presented a considerably bright red emission at 645 nm with a high QY of 51%, while the unmixed Au<sub>22</sub>(FGGC)<sub>18</sub> nanoclusters showed relatively weak red luminescence with a low QY of 7.5% under the same conditions. Fig. 3 shows that the luminescence intensity of FGGC-AuNCs was also remarkably enhanced upon adding 200 μL CB[8] at moderate concentrations. The maximum absolute quantum yield can reach as high as 39% at room temperature, which is also high for AuNCs in aqueous solutions. So far, only two reports on AuNCs with greater quantum yields than that of our AuNC system in aqueous solutions are available;<sup>45,46</sup> nevertheless, their maximum emissive wavelengths are both less than 550 nm. Our work endows the bright emissive AuNCs with long wavelength emission.

Different from the extreme variations in luminescence intensity, the UV-Vis absorption spectra of FGGC-AuNCs presented fewer changes with different amounts of CB[7] and a slight decline of absorption intensity upon adding increasing amounts of CB[8] (see Fig. S5†), indicating that the composition of nanoclusters and the energy level structure at the ground state remained unchanged for supramolecular assembled nanoclusters.

To demonstrate the role of supramolecular self-assembly in the emission enhancement of AuNCs, adamantylamine (ADA), an ideal competitive guest for CB[7]-based complexes, was selected to dissociate CB[7]/FGGC-AuNCs assemblies. As shown in Fig. 3c, the photo-luminescence intensity of CB[7]/FGGC-AuNCs falls dramatically compared to the intensity of unmixed FGGC-AuNCs (red dot in the inset diagram) upon adding sufficient ADA solution. Besides, different types of common cucurbiturils and their monomer glycoluril were also investigated for enhancing the emission of FGGC-AuNCs. Fig. 3d suggests that only CB[7] and CB[8] could apparently promote luminescence. CB[6] (considering the molecular size and availability, other CB[*n*] such as CB[10] and CB[14] were not used in this study) and glycoluril, which could hardly assemble with the FGGC peptide, exhibited no enhancement of the luminescence intensity of FGGC-AuNCs in aqueous solutions, further evidencing the crucial role of host-guest self-assembly to brighten FGGC-AuNCs.

### Size evolution of CB/FGGC-AuNC assemblies

Besides the optical variations, the size of FGGC-AuNCs would be changed as well when their surface is capped with CB[7] and CB[8]. The HRTEM images in Fig. 4a and b show that supramolecular CB[7]/FGGC-AuNCs presented a larger particle size (~2.5 nm) than FGGC-AuNCs (~1 nm) in aqueous solutions (the ratio of CB[7] is sufficient), which was ascribed to the CB[7] cap on the surface of nanoclusters. On the other hand, considering the spatial restriction of FGGC peptides on intra-nanoclusters, the 1:2 binding manner makes CB[8] act as a “crosslinker” for two FGGC ligands on inter-nanoclusters. Accordingly, Fig. 4c, d and S6† present an apparently enlarged size evolution of AuNCs with

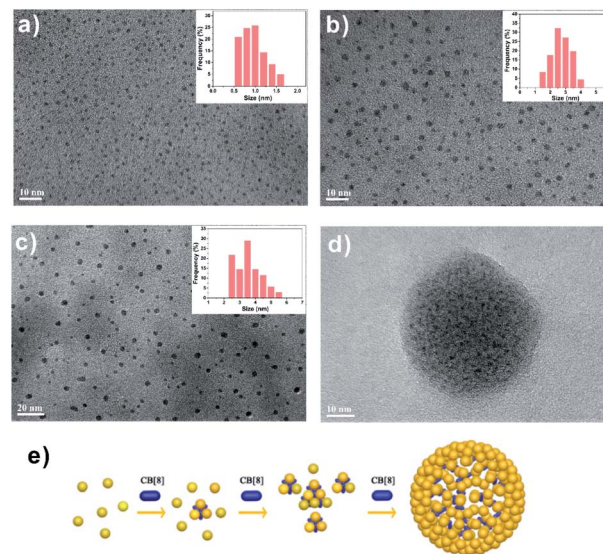


Fig. 4 HRTEM images of FGGC-AuNCs (a) and CB[7]/FGGC-AuNCs (b) in aqueous solutions. Inset: size distribution of AuNCs referring to TEM images. The ratio of CB[7] is in excess as evaluated by luminescence study. (c and d) Images showing high resolution TEM morphologies of FGGC-AuNCs (2 mL, the absorbance at 515 nm is 0.05) with different volumes of CB[8] aqueous solutions (0.1 mM): 200 μL (c) and 300 μL (d). Inset: size distribution of AuNCs referring to TEM images. (e) Schematic diagram of FGGC-AuNC assembly with different amounts of CB[8]. Yellow balls represent AuNCs.

addition of increasing amounts of CB[8], and the size evolution process is schematically described in Fig. 4e. As shown in Fig. S6,† a small amount of CB[8] (80 μL) could only crosslink some FGGC-AuNCs into larger ones. More nanoclusters are further crosslinked into larger particles of sizes ranging from 2.5 to 5.5 nm when 200 μL CB[8] is added (Fig. 4c). Notably, more CB[8] (300 μL) can further assemble these “big” nanoclusters into larger ones with diameters ranging from 30 to 80 nm (Fig. S6†), and it is easy to observe in Fig. 4d that small nanoclusters are embedded in a big nanoparticle with a size of 50 nm. To date, gold nanoclusters of different sizes have been less reported, and our host-guest strategy assisted by CB[8] shows a remarkable result to obtain highly emissive nanoclusters in large sizes. It’s worth noting that the nano size plays an important role in toxicity and cytosis of nanoparticles; this research may reveal a useful tool for investigations in nanobiology.

### Mechanism of emission enhancement for assembled CB/FGGC-AuNCs

For the traditional pure organic room temperature phosphorescence (RTP) system fabricated by host-guest self-assembly, macrocyclic hosts provide a rigid and oxygen-isolated environment by completely encapsulating guest luminophores into their rigid cavities. In our CB/FGGC-AuNC assemblies, the inclusion sites are at the outer end of FGGC ligands on the surface of nanoclusters; however, simple peptide ligands don’t contribute to the luminescence origin which has remained in dispute between “Au(0)-kernel emission” and “Au(i)-surface



emission" so far.<sup>33,39,42</sup> Nevertheless, surface surroundings and ligand types on the surfaces of gold nanoclusters have been demonstrated to be directly responsible for the luminescence intensity in previous studies.<sup>33,47,48</sup> In this respect, the better surface rigidity of supramolecular FGGC-AuNC assemblies with CB[7] and CB[8] is probably the major factor for the extreme emission enhancement. Compared with the loose FGGC peptide, CB/FGGC complexes are more rigid after host-guest self-assembly driven by the hydrophobic effect, ion-dipolar interaction, and H-bonds due to the following effects: (i) the movements of the phenylalanine unit are restricted by the rigid cavity of CB[7] and CB[8]; (ii) H-bonds between carbonyls on CB[n]s and amides on the peptide further suppress the flexibility; (iii) the large molecular mass and size of cucurbiturils (1192 Da, 9.1 Å height, and 16.0 Å outer diameter for CB[7]; 1329 Da, 9.1 Å height, and 17.5 Å outer diameter for CB[8]) restrict the motion of CB/FGGC ligands on the surface.

To confirm the above presumptions, the temperature dependent photoluminescence intensity of FGGC-AuNCs was investigated at temperatures ranging from 278 K to 338 K. Fig. 5 and S7† suggest that the luminescence intensity of both FGGC-AuNCs and CB[7]/FGGC-AuNCs decreased considerably when the temperature increased from 278 K to 338 K. Notably, as indicated in Fig. 5c, the decay tendency of CB[7]/FGGC-AuNCs with temperature was apparently different compared with that of the simple FGGC-AuNC solution. For FGGC-AuNCs, the emission intensity decreased dramatically in an exponential decay (the rate was  $0.0367\text{ K}^{-1}$  after normalization) with the temperature ranging from 278 K to 338 K; however, the supramolecular CB[7]/FGGC-AuNCs presented a linear and slower (decay rate was  $0.0087\text{ K}^{-1}$  after normalization) decay tendency under the same conditions. This result suggests that the flexible surfaces of FGGC-AuNCs can be fixed by CBs *via* host-guest interactions thus endowing them with stronger resistance to heat. It is worth noting that the disassembly of CB[7]/FGGC at 338 K could be neglected due to the large  $K_a$  and  $\Delta H$  value approximately evaluated using the Van't Hoff equation (the detailed calculations are presented in the ESI†). Furthermore, considering the contribution of H-bonds to the surface rigidity, we investigated the emission intensity of gold nanoclusters

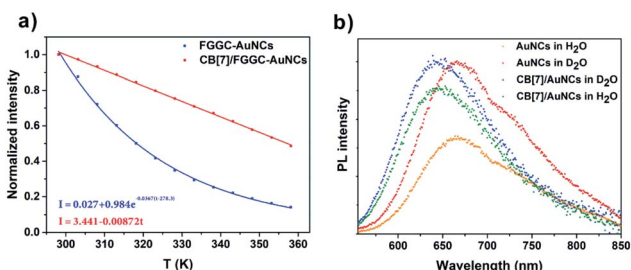


Fig. 5 (a) Maximum luminescence intensity variations and corresponding fitting curves and formulae of FGGC-AuNCs (blue) and CB[7]/FGGC-AuNCs (red) in aqueous solutions with temperature. (b) Photoluminescence spectra of FGGC-AuNCs and CB[7]/FGGC-AuNCs in H<sub>2</sub>O and D<sub>2</sub>O (95% V/V in H<sub>2</sub>O). All samples were excited at 515 nm.

after isotopic exchange of active hydrogens of the FGGC peptide in D<sub>2</sub>O. As shown in Fig. 5b, the luminescence intensities of two nanoclusters were apparently stronger in D<sub>2</sub>O than in H<sub>2</sub>O, suggesting that stronger H-bonds could effectively enhance the emission of FGGC-AuNCs through deuterating active hydrogens on amide and acid groups. Also, the luminescence intensity of FGGC-AuNCs exhibited greater sensitivity to D<sub>2</sub>O demonstrating that the ligands of FGGC-AuNCs were more flexible compared with those of CB[7]/FGGC-AuNCs in solutions.

To reveal the photodynamic information of the emission enhancement of supramolecular AuNCs in aqueous solutions, time-dependent luminescence decay traces of FGGC-AuNCs and CB[n]/FGGC-AuNCs were obtained by transient luminescence spectroscopy. As shown in Fig. 6 and S8,† both FGGC-AuNCs and CB[n]/FGGC-AuNCs presented long luminescence lifetimes only

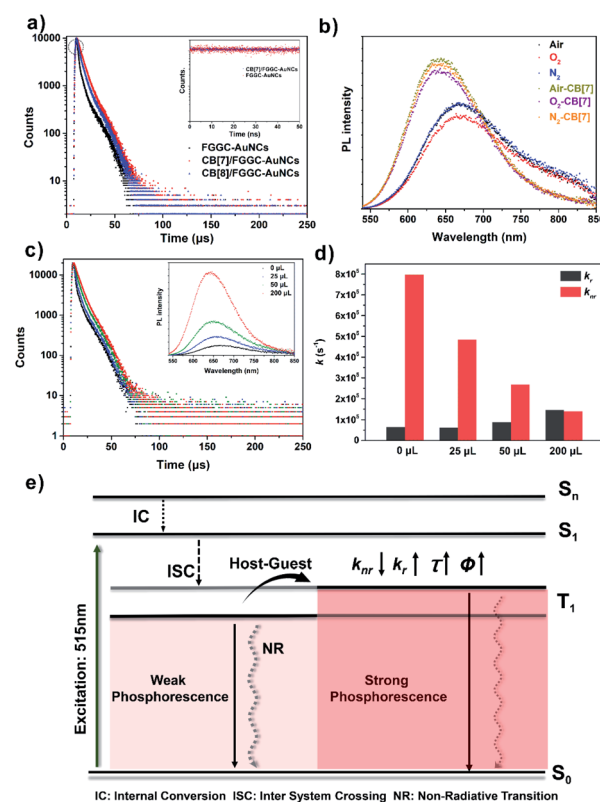


Fig. 6 (a) Luminescence decay of FGGC-AuNCs (black dots), CB[7]/FGGC-AuNCs (red dots) and CB[8]/FGGC-AuNCs (blue dots) in aqueous solutions at 640 nm. Inset: Luminescence decay of FGGC-AuNCs (red dots) and CB[7]/FGGC-AuNCs (blue dots) at 640 nm in the nanosecond range. The nanosecond luminescence decay traces covered a range from 5 ps to 50 ns. (b) Luminescence spectra of FGGC-AuNCs and CB[7]/FGGC-AuNCs under air, O<sub>2</sub>, and N<sub>2</sub> conditions. The preparation sequence of samples: no bubbling-O<sub>2</sub> bubbling-N<sub>2</sub> bubbling. (c and d) Transient luminescence spectra (c) and corresponding kinetic parameters (d) of FGGC-AuNCs with different volumes of CB[7] in aqueous solutions. The emission wavelength at 640 nm was selected to record the luminescence decay traces. Inset: Luminescence intensity of corresponding samples. All concentrations of FGGC-AuNC samples are identical (the absorbance at 515 nm is 0.03); CB[7] concentration: 1 mM. (e) Schematic diagram to illustrate the photodynamic procedure of emission enhancement of FGGC-AuNCs *via* host-guest self-assembly.



at the microsecond level, and the luminescence intensity declined under oxygen-rich conditions and then returned to the original intensity upon bubbling nitrogen. These results indicate that the luminescence of  $\text{Au}_{22}(\text{FGGC})_{18}$  nanoclusters involves triplet excited states. Referring to a previous study by Pyo *et al.* demonstrating that the emission intensity of  $\text{Au}_{22}$  nanoclusters varies negatively with temperatures below 150 K,<sup>39</sup> the long lifetime luminescence from FGGC-AuNCs should be further classified into phosphorescence with a high efficiency of intersystem crossing (ISC). Besides, Fig. 6a also shows longer luminescence lifetimes of FGGC-AuNCs after assembly with CB[7] and CB[8]. To reveal the detailed mechanism of this phenomenon, quantum yields and luminescence decay lifetimes of FGGC-AuNCs with different amounts of CB[7] (the detailed fitting parameters are listed in Table S1†) were investigated, and the rates of radiative transition ( $k_r$ ) and non-radiative transition ( $k_{nr}$ ) of the  $T_1$  state were obtained according to the following equations (assuming the efficiency of ISC is 100%):

$$k_{nr} + k_r = 1/\tau$$

$$k_r = \Phi(k_{nr} + k_r)$$

where  $\Phi$  represents the corresponding quantum yield. In Fig. 6c, S9 and Table S2,† the luminescence quantum yield increased from 7.5% to 51% and lifetime increased from 1.61  $\mu\text{s}$  to 3.51  $\mu\text{s}$  when a sufficient amount of CB[7] was added. Accordingly, the non-radiative transition rate  $k_{nr}$  rapidly decreased from  $7.97 \times 10^5 \text{ s}^{-1}$  to  $1.40 \times 10^5 \text{ s}^{-1}$  and the radiative transition  $k_r$  increased from  $6.4 \times 10^4 \text{ s}^{-1}$  to  $1.45 \times 10^5 \text{ s}^{-1}$ . Therefore, the rigidified FGGC-AuNCs *via* host-guest self-assembly can contribute to the promotion of radiative transition and suppression of non-radiative processes simultaneously, and the suppression of non-radiative processes is the major factor in the large emission enhancement of CB/FGGC-AuNCs. It is worth noting that this suppression of non-radiative transition *via* host-guest self-assembly is fairly similar to the aggregation-induced emission (AIE) mechanism by which luminescence can be enhanced through a restriction of the intramolecular motion of parts of luminophores.<sup>47,48</sup>

### Live cell imaging using CB[7]/FGGC-AuNCs

The bright, large Stokes shift and long wavelength emission makes CB[7]/FGGC-AuNCs an excellent candidate for live cell imaging. To this end, we treated human lung adenocarcinoma cells (A549 cells) without and with CB[7]/FGGC-AuNCs ( $5 \mu\text{g mL}^{-1}$ ) for 6 hours and stained the nuclei with the nuclear counterstain DAPI. Then confocal laser scanning microscopy (CLSM) was used to investigate the results of living cell imaging. In Fig. 7, the A549 cells with CB[7]/FGGC-AuNCs showed apparent red emission (detected from 600 nm to 750 nm) located in the cytoplasm under laser irradiation at 515 nm with clear blue emission (detected from 440 nm to 480 nm) from DAPI in cell nuclei under excitation at 405 nm. In contrast, the A549 cells without CB[7]/FGGC-AuNCs presented solely blue emissions of DAPI in the nucleus, showing the excellent result of highly emissive CB[7]/FGGC-AuNCs in live cell imaging.

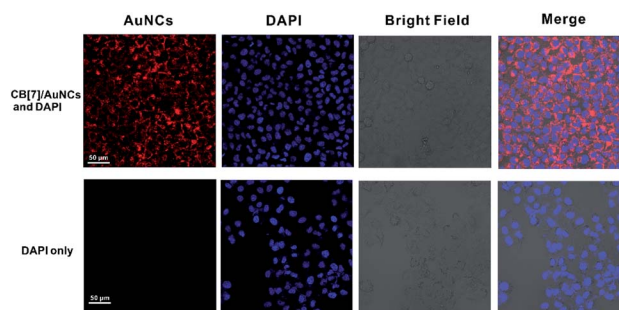


Fig. 7 CLSM photographs of A549 cells treated with CB[7]/FGGC-AuNCs. The irradiation laser is at 515 nm and detected wavelength range is from 600 nm to 750 nm for imaging A549 cancer cells with (up) and without (down) incubation with CB[7]/FGGC-AuNCs ( $5 \mu\text{g mL}^{-1}$ ) for 6 h. The nuclei were stained with DAPI (excitation laser: 405 nm, detected wavelength range: 440–480 nm).

## Conclusions

In summary, we have developed a supramolecular self-assembly approach to reversibly brighten and enlarge the emissive  $\text{Au}_{22}(\text{FGGC})_{18}$  nanoclusters assisted by host-guest assembly between CB[*n*] ( $n = 7, 8$ ) and FGFC peptides in aqueous solutions. The strategy of host-guest self-assembly can effectively enhance the emission of AuNCs *via* rigidifying the surface of nanoclusters, resulting in an effective suppression of non-radiative transition and promotion of radiative transition demonstrated by ultrafast spectroscopy study. The red luminescence of the self-assembled gold nanoclusters presented a high QY of 39% for CB[8] and 51% for CB[7] in aqueous solutions and is one of the strongest red emissions from AuNCs in aqueous solutions. Such supramolecular AuNCs exhibit excellent results in live A549 cancer cell luminescence imaging. Besides the considerably enhanced emission, FGFC-AuNCs can be crosslinked non-covalently into large nanoparticles with a size of tens of nanometers by CB[8], providing a feasible approach for constructing size-adjustable emissive nanoparticles. In addition, our study expands the frontier of host-guest self-assembly on ultrasmall nano-size scales and provides a facile and non-covalent means for further exploring the luminescence mechanism and other properties such as catalysis and nano-metabolism of gold nanoclusters.

## Conflicts of interest

There are no conflicts to declare.

## Acknowledgements

This report was financially supported by the National Natural Science Foundation of China (21788102, 21722603 and 21871083), Shanghai Municipal Science and Technology Major Project (Grant No. 2018SHZDZX03), 'Shu Guang' project supported by the Shanghai Municipal Education Commission and Shanghai Education Development Foundation (19SG26), Innovation Program of Shanghai Municipal Education Commission



(2017-01-07-00-02-E00010) and Fundamental Research Funds for the Central Universities. The authors gratefully acknowledge Prof. Yujian Zhang (Huzhou University) for his kind assistance in measuring quantum yield, Dawei Jiang for the help in cancer cell culture, and Dr Yifan Gong (Fudan University) for the help in recording transient luminescence spectra.

## References

- H. Wang, C. N. Zhu, H. Zeng, X. Ji, T. Xie, X. Yan, Z. L. Wu and F. H. Huang, *Adv. Mater.*, 2019, **31**, 1807328.
- Y. Chen, F. H. Huang, Z. T. Li and Y. Liu, *Sci. China: Chem.*, 2018, **61**, 979–992.
- C. L. Sun, H. Q. Peng, L. Y. Niu, Y. Z. Chen, L. Z. Wu, Z. H. Tung and Q. Z. Yang, *Chem. Commun.*, 2018, **54**, 1117–1120.
- A. W. Heard and S. M. Goldup, *ACS Cent. Sci.*, 2020, **6**, 117–128.
- Q. W. Zhang, D. Li, X. Li, P. B. White, J. Mecinović, X. Ma, H. Ågren, R. J. M. Nolte and H. Tian, *J. Am. Chem. Soc.*, 2016, **138**, 13541–13550.
- B. Tang, W. L. Li, Y. Jiao, J. B. Lu, J. F. Xu, Z. Q. Wang, J. Li and X. Zhang, *Chem. Sci.*, 2018, **9**, 5015–5020.
- H. Chen, X. Zeng, H. P. Tham, S. Z. F. Phua, W. Cheng, W. Zeng, H. Shi, L. Mei and Y. Zhao, *Angew. Chem., Int. Ed.*, 2019, **58**, 7641–7646.
- S. J. Pike, E. Lavagnini, L. M. Varley, J. L. Cook and C. A. Hunter, *Chem. Sci.*, 2019, **10**, 5943–5951.
- S. J. Barrow, S. Kaser, M. J. Rowland, J. del Barrio and O. A. Scherman, *Chem. Rev.*, 2015, **115**, 12320–12406.
- Y. Wu, D. U. Shah, B. Wang, J. Liu, X. Ren, M. H. Ramage and O. A. Scherman, *Adv. Mater.*, 2018, **30**, 1707169.
- X. Ma, J. Wang and H. Tian, *Acc. Chem. Res.*, 2019, **52**, 738–748.
- S. He, F. Biedermann, N. Vankova, L. Zhechkov, T. Heine, R. E. Hoffman, A. De Simone, T. T. Duignan and W. M. Nau, *Nat. Chem.*, 2018, **10**, 1252–1257.
- Z. Hirani, H. F. Taylor, E. F. Babcock, A. T. Bockus, C. D. Varnado Jr, C. W. Bielawski and A. R. Urbach, *J. Am. Chem. Soc.*, 2018, **140**, 12263–12269.
- Y. Jang, M. Jang, H. Kim, S. J. Lee, E. Jin, J. Y. Koo, I.-C. Hwang, Y. Kim, Y. H. Ko, I. Hwang, J. H. Oh and K. Kim, *Chem*, 2017, **3**, 641–651.
- N. Dong, J. He, T. Li, A. Peralta, M. R. Avey, M. Ma and A. E. Kaifer, *J. Org. Chem.*, 2018, **83**, 5467–5473.
- H. Zhang, J. R. Wu, X. Wang, X. S. Li, M. X. Wu, F. Liang and Y. W. Yang, *Dyes Pigm.*, 2019, **162**, 512–516.
- G. Qu, Y. Zhang and X. Ma, *Chin. Chem. Lett.*, 2019, **30**, 1809–1814.
- E. Scalise, V. Srivastava, E. M. Janke, D. Talapin, G. Galli and S. Wippermann, *Nat. Nanotechnol.*, 2018, **33**, 841–848.
- P. D. Jadzinsky, G. Calero, C. J. Ackerson, D. A. Bushnell and R. D. Kornberg, *Science*, 2007, **318**, 430–433.
- N. A. Sakthivel and A. Dass, *Acc. Chem. Res.*, 2018, **51**, 1774–1783.
- Y. Du, H. Sheng, D. Astruc and M. Zhu, *Chem. Rev.*, 2020, **120**, 526–622.
- J. Zheng, J. T. Petty and R. M. Dickson, *J. Am. Chem. Soc.*, 2003, **125**, 7780–7781.
- T. Jiang, X. Wang, J. Wang, G. Hu and X. Ma, *ACS Appl. Mater. Interfaces*, 2019, **11**, 14399–14407.
- H. Zhang, H. Liu, Z. Tian, D. Lu, Y. Yu, S. Cestellos-Blanco, K. K. Sakimoto and P. Yang, *Nat. Nanotechnol.*, 2018, **13**, 900–905.
- T. Higaki, Y. Li, S. Zhao, Q. Li, S. Li, X. S. Du, S. Yang, J. Chai and R. Jin, *Angew. Chem., Int. Ed.*, 2019, **58**, 8291–8302.
- M. Zhou, T. Higaki, G. Hu, M. Y. Sfeir, Y. Chen, D. E. Jiang and R. Jin, *Science*, 2019, **364**, 279–282.
- L. Shang, F. Stockmar, N. Azadfar and G. U. Nienhaus, *Angew. Chem., Int. Ed.*, 2013, **52**, 11154–11157.
- M. Yu, J. Xu and J. Zheng, *Angew. Chem., Int. Ed.*, 2019, **58**, 4112–4128.
- Y. Zheng, L. Lai, W. Liu, H. Jiang and X. Wang, *Adv. Colloid Interface Sci.*, 2017, **242**, 1–16.
- G. Gao, R. Chen, M. He, J. Li, J. Li, L. Wang and T. Sun, *Biomaterials*, 2019, **194**, 36–46.
- B. J. Du, X. Y. Jiang, A. Das, Q. H. Zhou, M. X. Yu, R. C. Jin and J. Zheng, *Nat. Nanotechnol.*, 2017, **12**, 1096–1102.
- D. Li, Z. Chen and X. Mei, *Adv. Colloid Interface Sci.*, 2017, **250**, 25–39.
- Q. Li, M. Zhou, W. Y. So, J. Huang, M. Li, D. R. Kauffman, M. Cotlet, T. Higaki, L. A. Peteanu, Z. Shao and R. Jin, *J. Am. Chem. Soc.*, 2019, **141**, 5314–5325.
- S. Wang, X. Meng, A. Das, T. Li, Y. Song, T. Cao, X. Zhu, M. Zhu and R. Jin, *Angew. Chem., Int. Ed.*, 2014, **53**, 2376–2380.
- L. He, Z. Gan, N. Xia, L. Liao and Z. Wu, *Angew. Chem., Int. Ed.*, 2019, **58**, 9897–9901.
- Z. Wu and R. Jin, *Nano Lett.*, 2010, **10**, 2568–2573.
- Z. Wu, Y. Du, J. Liu, Q. Yao, T. Chen, Y. Cao, H. Zhang and J. Xie, *Angew. Chem., Int. Ed.*, 2019, **58**, 8139–8144.
- S. E. Crawford, C. M. Andolina, A. M. Smith, L. E. Marbella, K. A. Johnston, P. J. Straney, M. J. Hartmann and J. E. Millstone, *J. Am. Chem. Soc.*, 2015, **137**, 14423–14429.
- K. Pyo, V. D. Thanthirige, K. Kwak, P. Pandurangan, G. Ramakrishna and D. Lee, *J. Am. Chem. Soc.*, 2015, **137**, 8244–8250.
- Y. Yu, Z. Luo, D. M. Chevrier, D. T. Leong, P. Zhang, D. E. Jiang and J. Xie, *J. Am. Chem. Soc.*, 2014, **136**, 1246–1249.
- Y. Pei, J. Tang, X. Tang, Y. Huang and X. C. Zeng, *J. Phys. Chem. Lett.*, 2015, **6**, 1390–1395.
- K. L. D. M. Weerawardene, E. B. Guidez and C. M. Aikens, *J. Phys. Chem. C*, 2017, **121**, 15416–15423.
- H. D. Nguyen, D. T. Dang, J. L. van Dongen and L. Brunsveld, *Angew. Chem., Int. Ed.*, 2010, **49**, 895–898.
- X. X. Tan, L. L. Yang, Y. L. Liu, Z. H. Huang, H. Yang, Z. Q. Wang and X. Zhang, *Polym. Chem.*, 2013, **4**, 5378–5381.
- H. H. Deng, X. Q. Shi, F. F. Wang, H. P. Peng, A. L. Liu, X. H. Xia and W. Chen, *Chem. Mater.*, 2017, **29**, 1362–1369.
- J. Zheng, C. Zhang and R. M. Dickson, *Phys. Rev. Lett.*, 2004, **93**, 077402.
- W. Z. Yuan and Y. Zhang, *J. Polym. Sci., Part A: Polym. Chem.*, 2017, **55**, 560–574.
- J. Mei, N. L. C. Leung, R. T. K. Kwok, J. W. Y. Lam and B. Z. Tang, *Chem. Rev.*, 2015, **115**, 11718–11940.

